Bioorganic & Medicinal Chemistry xxx (2014) xxx–xxx

Contents lists available at ScienceDirect

Bioorganic & Medicinal Chemistry

journal homepage: www.elsevier.com/locate/bmc

Influence of azide incorporation on binding affinity by small papain inhibitors

Angelique E. M. Wammes [a], Tom G. Hendriks [a,b], Helene I. V. Amatdjais-Groenen [a], Marloes A. Wijdeven [a], Jan C. M. van Hest [a], Floris L. van Delft [a], Tina Ritschel [b,*], Floris P. J. T. Rutjes [a,*]

[a] Radboud University Nijmegen, Institute for Molecules and Materials, Heyendaalseweg 135, 6525 AJ Nijmegen, The Netherlands
[b] Computational Discovery and Design (CDD) Group, Centre for Molecular and Biomolecular Informatics (CMBI), Radboud University Medical Center, PO Box 9101, 6500 HB Nijmegen, The Netherlands

ARTICLE INFO

Article history:
Received 15 April 2014
Revised 28 May 2014
Accepted 1 June 2014
Available online xxxx

Keywords:
Azides
Strain-promoted cycloaddition
Papain inhibitors
Biosensors
Docking study

ABSTRACT

In order to develop affinity-based biosensor platforms, appropriate ligands with a functional handle for immobilization onto a biosensor surface are required. To this end, a library of papain inhibitors was designed and synthesized, containing different azide linkers for subsequent immobilization by 'click' chemistry, in this particular case by copper-free, strain-promoted azide–alkyne cycloaddition (SPAAC). Furthermore, a molecular docking study was performed to obtain a better insight as to at which position such azide handles could be tolerated without affecting binding affinity. Although the azide moiety is small, in some cases its introduction strongly influenced the binding affinity. For one class of inhibitors a swapped binding mode was proposed to explain the results. In addition, a specific site for linker introduction was identified, which did not significantly affect the binding affinity.

1. Introduction

Biosensors, analytical devices to detect the presence of a specific biomolecule in a natural sample, have become an essential tool in medicinal, forensic and environmental analysis.[1,2] In general, a biosensor consists of two main components, namely a recognition element and a transducer element: the recognition element ensures detection of the target structure (the analyte) by a binding event, while the transducer element signals the binding to a device for read-out. To obtain a sensitive and selective biosensor, it is important to construct a recognition element that provides a stable interface for interaction between the target biomolecules and the immobilized binding partners (ligands), which are packed with optimal density. Conceptually, immobilization of a ligand to the surface of a biosensor requires the prior installment of a suitable linking moiety or handle. Although typically small, it must be taken into consideration that such a handle may compromise binding of the ligand to the analyte, for example due to steric bulk or unspecific hydrophobic interactions. Hence, a judicious choice of the handle, as well as the site of attachment on the ligand is required. The interface should furthermore be insensitive to non-specific binding interactions. Commonly established tools for immobilization include non-covalent streptavidin–biotin interaction, covalent attachment by amide coupling or so-called 'click' chemistry.[3] One powerful example of the latter approach is the strain-promoted azide–alkyne cycloaddition (SPAAC), that is, reaction between an azide and a strained alkyne, typically a cyclooctyne.[4–9] Although the linker is generally small, it can significantly compromise the requisite binding of the ligand to the analyte. This again requires a deliberate choice for a specific linker, as well as the site of attachment.

To investigate the influence of the incorporation of the azide moiety, a biosensor for exotic fruit allergen detection was used as a model system. We chose to work with papain, a cysteine protease present in papaya fruit, which has been studied previously in our group for enzymatic amide bond formation.[10–12] Furthermore, papain is a good model protein for exotic fruit allergens, since its active site shows great homology with the allergens found in, for example, kiwi and pineapple. Thus, a set of potential new inhibitors (**3**–**5**) for papain was designed and synthesized based on compounds which are known to inhibit the enzyme (Fig. 1, compounds **1** and **2**).[13]

The cysteine proteases of the papain superfamily display relatively broad substrate specificity. As a result, designing inhibitors that are highly selective for papain has proven to be a challenging task.[14] To date, a variety of inhibitors have been developed with

* Corresponding authors. Tel.: +31 24 3619674 (T.R.); tel.: +31 24 3653202; fax: +31 24 3653393 (F.P.J.T.R.).
E-mail addresses: tina.ritschel@radboudumc.nl (T. Ritschel), f.rutjes@science.ru.nl (F.P.J.T. Rutjes).

http://dx.doi.org/10.1016/j.bmc.2014.06.001
0968-0896/

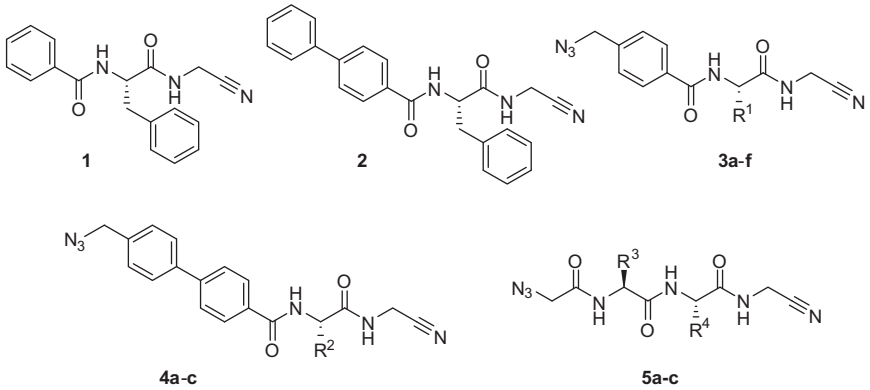

Figure 1. Peptidonitriles **1** and **2** are known papain inhibitors.[13] Compound **3**: **a** R^1 = iBu (Leu), **b** R^1 = *n*-Bu (Nle), **c** R^1 = Bn (Phe), **d** $R^1 = CH_2C_6H_4OH$ (Tyr), **e** $R^1 = (CH_2)_2Ph$ (*h*-Phe), **f** $R^1 = (CH_2)_2C_6H_4OH$ (*h*-Tyr); **4**: **a** R^2 = *n*-Bu (Leu), **b** R^2 = Bn (Phe), **c** $R^2 = CH_2C_6H_4OH$ (Tyr); **5**: **a** R^3 = iBu (Leu), R^4 = iBu (Leu); **b** R^3 = iBu (Leu), R^4 = Bn (Phe); **c** R^3 = Bn (Phe), R^4 = Bn (Phe).

different binding functionalities,[13,15–18] but for this research in particular nitrile-containing peptides were designed for interaction in the active site of papain. Crucial in the design was to preserve the inhibition properties by introducing the azide linker in a position where the binding to papain was not disturbed.

The designed inhibitors were synthesized and tested in an enzymatic assay. Furthermore, the binding mode was analyzed using molecular docking studies. The predicted binding modes of the inhibitors were reviewed, which led to a better understanding of the structure activity relationships.

2. Results and discussion

2.1. Synthesis

Synthesis of the ligands started with the incorporation of a nitrile functional group by coupling of aminoacetonitrile to the *N*-Boc-protected amino acids **6a–f** with the mixed anhydride method (Scheme 1). Thus, isobutyl chloroformate was added to the *N*-Boc-protected amino acid in the presence of freshly distilled triethylamine and THF as solvent, leading to compounds **7a–f** in moderate to good yields. Subsequent Boc deprotection was performed with TFA in THF/water (1:1 v/v) to afford compounds **8a–f** in (near) quantitative yields.

The next step involved the incorporation of an azido-containing benzoyl or 4-phenylbenzoyl moiety at the N-terminus. The required 4-azidomethylbenzoic acid (**9**) was readily obtained by nucleophilic substitution of 4-bromomethylbenzoic acid, using a literature procedure (not depicted).[19] The synthesis of biphenyl derivative **10**, however, proved to be more troublesome (Scheme 2). Synthesis in this case started with a palladium-catalyzed Suzuki coupling of 4-bromobenzyl alcohol (**11**) with boronic acid derivative **12**. Although a yield of only 24% was attained, sufficient material was obtained to proceed so that no further optimization was performed. The Suzuki coupling was followed by azide substitution of the hydroxyl group via the corresponding mesylate, leading to biphenyl ester **14** in 98% yield. Subsequent saponification provided the desired 4-[4-(azidomethyl)phenyl]benzoic acid derivative **10** in quantitative yield. Coupling of 4-azidomethylbenzoic acid (**9**) to compounds **8a–f** was performed under standard amide coupling conditions using EDC in the presence of HOBt (Scheme 1), providing the desired benzoylated compounds **3a–f** in moderate to good yields. Introduction of biphenyl derivative **10** was performed under the same conditions, however, products **4a**, **c** and **d** were obtained in low yields due to incomplete conversion and solubility issues during workup and purification. Nevertheless, sufficient material was obtained to perform binding studies with papain.

The synthesis of compounds **5a–c** commenced with peptide coupling of nitriles **8a** and **c** with Boc-protected leucine (**6a**) or phenylalanine (**6c**) to obtain compounds **15a–c** in moderate yield (Scheme 3). Boc deprotection was performed as described above, yielding compounds **16a–c** in quantitative yield. In this case, the azide moiety was incorporated by acylation of nitriles **16a–c** with azidoacetic acid, yielding azides **5a–c** in acceptable yields.

In the anticipated final situation as in a biosensor, where the ligands are immobilized on a surface, the azide will no longer exist as such, but will be converted into a triazole moiety. We therefore also evaluated the influence of such a transformation on binding affinity by synthesis of compounds **17** and **18**, involving SPAAC modification with two different strained cyclooctynes, namely BCN[8] and DIBAC.[5] Both triazoles **17**[9] and **18** were obtained in good yield starting from nitrile **3c** by stirring in MeOH in the presence of the cyclooctyne (Scheme 4). Due to the asymmetry in the cyclooctyne, **18** was obtained as an unseparable mixture of 1:1 triazole regioisomers.

2.2. Enzymatic evaluation

After successful synthesis of the library, dipeptide nitriles **3a–f**, **4a**, **c**, **d** and **5a–c** were evaluated for their papain affinity and the influence of the azide on the inhibitory properties. Our library was evaluated based on IC_{50} values obtained from a competitive UV assay.

Schechter and Berger introduced comprehensive nomenclature to describe the interaction between a peptide (P), the enzyme's substrate, and the enzyme recognition subsites (S).[20] This nomenclature is exemplified in Figure 2 for leupeptin, a tripeptide natural ligand for papain featuring an aldehyde function at the C-terminal arginine.[21] The S_1 pocket of papain is poorly defined as becomes clear from Figure 2b (arginine side-chain on the far right) and the arginine from leupeptin is solvent-exposed. The S_2 pocket is a hydrophobic pocket defined by Val133, Ala160 and Pro68 and the S_3 binding pocket is formed by two aromatic groups, Tyr61 and Tyr67.

2.2.1. Benzoyl ligands

The IC_{50} value for benzoyl ligand **1** was 0.36 ± 0.06 μM, which remained nearly the same for the azidomethylated derivative ligand **3c** (Table 1, entries 1 and 5). As expected for benzoyl compound **3d**, replacing phenylalanine by tyrosine had little influence on the IC_{50} value either (Table 1, entries 5 and 6). The homophenylalanine- and homotyrosine-derived ligands **3e** and **3f**, showed somewhat reduced binding affinity (Table 1, entries 7 and 8), as a potential indication that the side chains of homophenylalanine

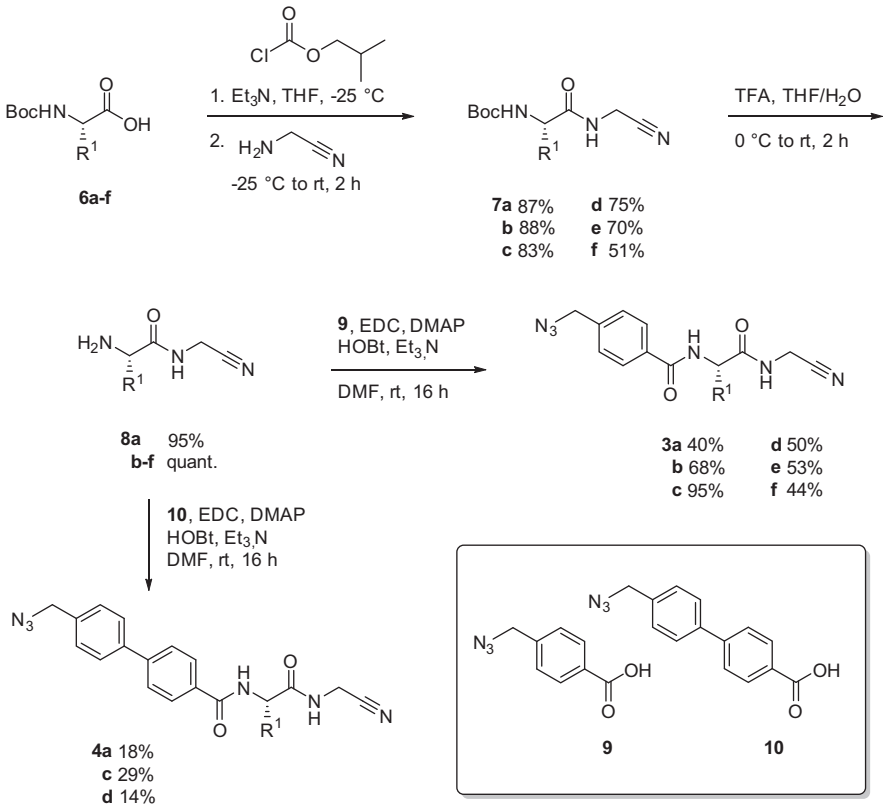

Scheme 1. Synthesis of papain ligands **3a**–**f** and **4a**,**c** and **d**; **a** = Leu, **b** = Nle, **c** = Phe, **d** = Tyr, **e** = *h*-Phe, **f** = *h*-Tyr.

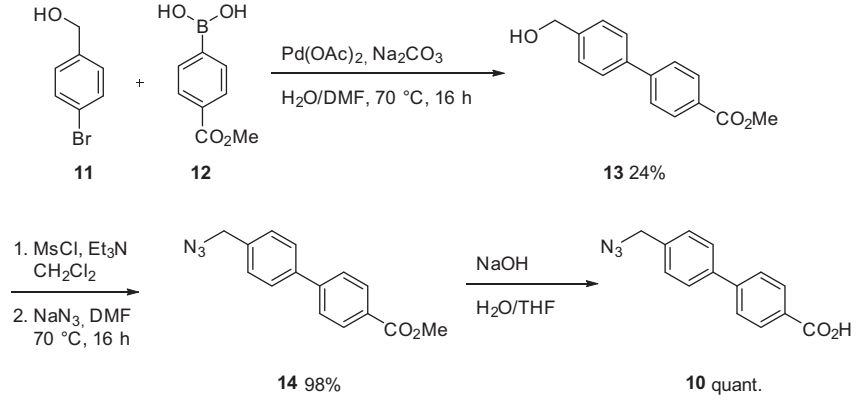

Scheme 2. Synthesis of biphenyl derivative **10**.

and homotyrosine are too long to properly fit in the S_3 site of papain. Replacing the aromatic side chain by non-aromatic hydrophobic side chains (Table 1, entries 3 and 4) reduced the binding affinity as well, possibly due to a lack of π–π interactions between the aromatic amino acids in the S_3 binding pocket and the aromatic side chains of ligands **3c** and **d**.

2.2.2. Phenylbenzoyl ligands

Literature compound **2** showed an IC_{50} value of 0.22 ± 0.07 μM (Table 1, entry 1). In contrast to the benzoyl derivatives described earlier, in this case introduction of the azidomethyl moiety directly at the aromatic ring, as in ligands **4a**–**c**, strongly decreased the inhibitory capacity (Table 1, entries 9–11). Surprisingly, after the introduction of the azidomethyl moiety, despite its small size, the S_3 binding pocket is no longer able to accommodate the aromatic site chain. No adequate explanation could be given at this point.

2.2.3. Leupeptin-based ligands

In the last class of inhibitors, the ligands **5a**–**c** (Table 1, entries 12–14), the azide was introduced on the N-terminus by azidoacetylation. The design of ligands **5a**–**c** was inspired by the structure of leupeptin, which features an N-acetylated tripeptide (Leu-Leu-Arg) with a reactive C-terminal functionality (aldehyde). To our surprise, all three ligands **5a**–**c** displayed IC_{50} values in the μM range, a 10-fold reduced affinity for papain compared to ligand **3c**. Apparently, replacement of the *N*-benzoyl group as in **3c** is not counterbalanced by the addition of an additional amino acid as in **5a**–**c**, despite the apparent larger similarity of the latter to leupeptin.

2.2.4. Triazole derivatives

The influence of the strained-alkynes was evaluated with triazoles **17** and **18** (Table 1, entries 15 and 16). Entry 15 showed that the triazole product resulting from reaction with BCN did not

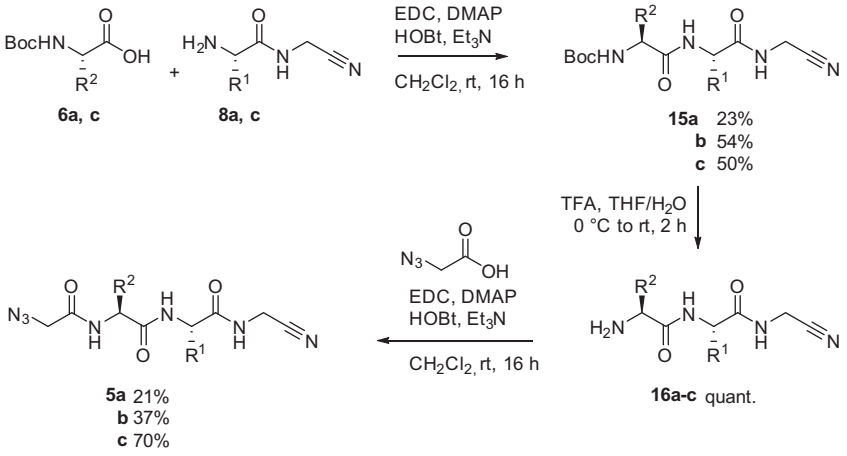

Scheme 3. Synthesis of leupeptin-based nitrile-containing papain ligands **5a–c**; **a** = $R^1 = R^2 =$ *i*Bu (Leu); **b** R^1 = Bn (Phe), R^2 = *i*Bu (Leu); **c** $R^1 = R^2$ = Bn (Phe).

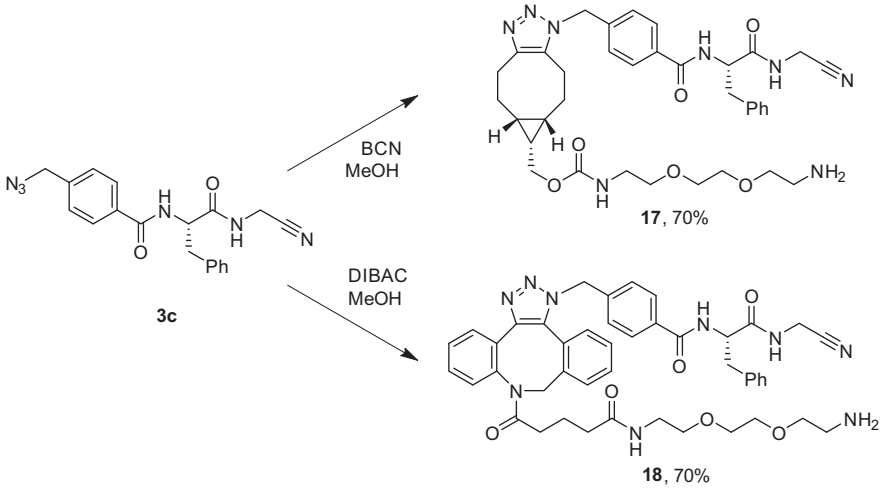

Scheme 4. Synthesis of cycloadducts **17** and **18**.

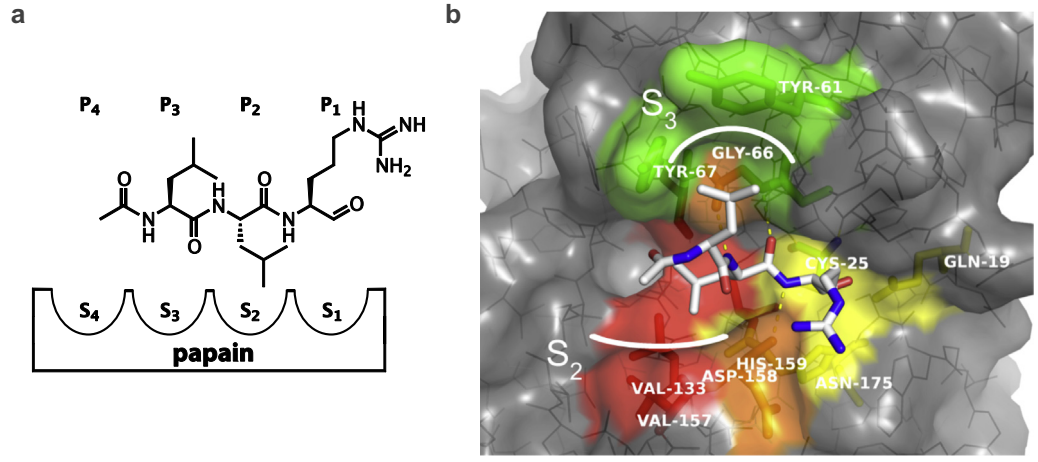

Figure 2. (a) General structure of nitrile-based peptide inhibitor and papain subpockets (S_1–S_4). The active site is described according to Schechter and Berger.[20] (b) Docking of leupeptin in the active site of papain (PDB file 1POP).

significantly influence the binding affinity, but on the other hand the more bulky DIBAC-derived triazole **18** had a strong impact (entry 16). Obviously, the triazole-DIBAC moiety is relatively large with respect to the small nitrile ligands and it was observed for the phenylbenzoyl ligands that the introduction of a small azide could already influence the binding affinity. Fortunately, the product

Table 1
IC_{50} values found for papain ligands **1**–**5**, **17** and **18**

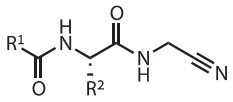

Entry	R^1	R^2	Compound	IC_{50} (μM)
1			**1**	0.36 ± 0.06
2	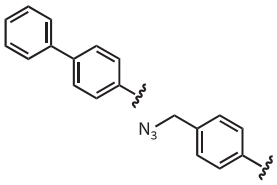		**2**	0.22 ± 0.07
3			**3a**	2.27 ± 0.3
4			**3b**	7.1 ± 3.2
5			**3c**	0.27 ± 0.03
6		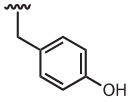	**3d**	0.28 ± 0.03
7		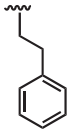	**3e**	0.71 ± 0.15
8		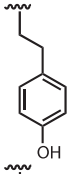	**3f**	0.98 ± 0.22
9	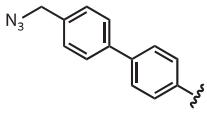		**4a**	1.58 ± 0.44
10			**4b**	13.9 ± 11.3
11		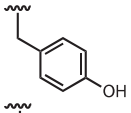	**4c**	51.16 ± 25.6
12	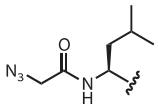		**5a**	2.71 ± 0.2
13			**5b**	2.25 ± 0.7
14	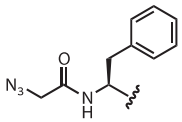		**5c**	3.97 ± 0.3

(*continued on next page*)

Table 1 (*continued*)

Entry	R^1	R^2	Compound	IC_{50} (μM)
15	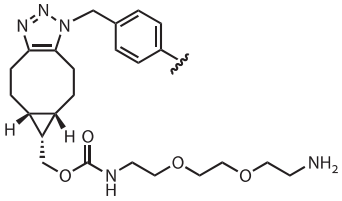		**17**	0.35 ± 0.08
16	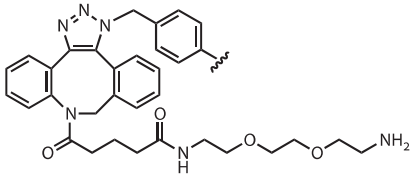		**18**	5.98 ± 1.9

resulting from SPAAC with BCN, a triazole–cyclooctyne 'click-product' appeared an excellent ligand for papain and is therefore clearly the cyclooctyne of choice.

2.3. Molecular modeling studies

Docking studies were performed to understand the results obtained in the enzymatic assay. The docking program Fleksy was used in this study, because it provides the option to treat parts of the protein in a flexible manner and at the same time allows induced fit adaptations of the protein upon inhibitor binding.[22] The induced fit model considers the initial binding event as relatively weak, but upon binding of the ligand to the protein, the protein can rapidly induce conformational changes to strengthen the ligand–protein binding.[23] The introduced inhibitors (Fig. 1, compounds **1**–**5**) bind covalently to Cys25 of papain, which provides valuable information of how the inhibitors will be oriented in the binding site and reduces the complexity of the docking process. Covalent docking with Fleksy is not directly possible. In order to simulate a covalent docking in Fleksy the position of the anchor fragment can be provided. In a first phase, a preselected base or anchor fragment of the ligand is placed into the active site independently of the rest of the ligand. In the second phase the remaining fragments of the ligand are added to the initially placed anchor fragment. As base fragment the C-terminal amide bond was chosen, based on the crystal structure of leupeptin in complex with papain (Fig. 3, red part of structure).[21] Prior to docking we investigated different papain structures of the PDB to explore different ligand–papain complexes, as well as the flexibility of the protein in the area of the binding site.

2.3.1. 3D-protein structure alignment

In order to investigate the variability of the S_2 and S_3 subsites among different ligand-papain complexes, a structural alignment was performed first, based on the α-carbons of 23 PDB-structures of papain (Fig. 4).[24] No large structural differences were found and therefore only little flexibility in the S_2 and S_3 subsites can be expected. Two tyrosines, Tyr61 and Tyr67, that determine the size of the S_3 pocket, appear to have some conformational freedom. Only the flexibility of the S_2 and S_3 subsites was examined, since at the P_1 position of all ligands a glycine is present and the S_4 pocket will not be occupied by our designed ligands.

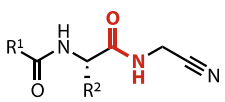

Figure 3. In red the anchor fragment used for Fleksy.

2.3.2. Docking

In order to evaluate the effect of an azide at different positions of the known inhibitors, one representative inhibitor of the three different ligand subclasses (Fig. 1, compounds **3c**, **4b** and **c**) was docked into the papain crystal structure PDB-code 1POP first. The best-scored pose of each docked inhibitor is shown in Figure 3. The covalent binding of the inhibitor to papain was mimicked during the docking process by fixing the position of the C-terminal amide bond as anchor fragment (Fig. 3). With this approach, the number of possible inhibitor orientations in the binding site was reduced, at the same time increasing the likelihood that the obtained docking poses are representative for the native binding mode. Besides the covalent nitrile–cysteine bond, all inhibitors depicted in Figure 1 are predicted to form three hydrogen bonds between their backbone and the backbone of the protein (Gly66 and Asp156), as already observed in the papain–leupeptin complex. Since the side chains of the amino acids of papain were treated to be flexible during the docking process, the final position of the side chains after docking can differ from the ones found in the crystal structure. In Figure 5, the changes of the side chains upon docking are shown for the amino acids that constitute the S_2 and S_3 binding site of papain. For example, in Figure 1d the side chains of Tyr61 and Tyr67 have moved aside to open up the S_3 binding site and allow the ligand to bind between the two tyrosine side chains.

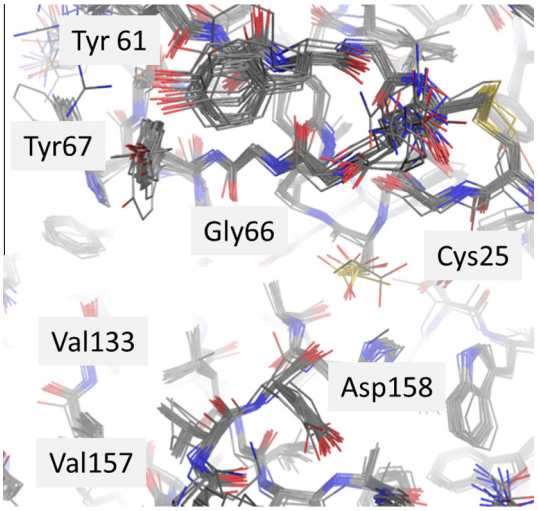

Figure 4. Structure alignment of 23 papain PBD structures.[24]

For each ligand subclass, the influence of the azide moiety will be separately discussed below, based on the docking results.

2.3.3. Benzoyl ligands

As established by the enzymatic assay, the introduction of the *p*-azidomethyl group did not significantly change the binding affinity (Table 1, entries 1 and 5). In Figure 5b, the best-scored docking orientation of benzoyl compound **1** was superposed to the papain–leupeptin complex. The introduction of the azide linker (as in inhibitor **4c**, Fig. 5c) at this position seemed to lead to negligible interference with the binding mode of the inhibitor.

Replacing the phenylalanine in position P_2 by an amino acid with another side chain was found to induce changes in binding affinity. With respect to the docking results it can be concluded that the best fit of the S_2 pocket is a phenylalanine. A minor reduction in binding affinity was observed for a tyrosine (ligand **4d**) and a large decrease in binding affinity was found for aliphatic moieties (ligands **4a**, **b**).

Two non-natural amino acids, *homo*-phenylalanine and *homo*-tyrosine, were introduced at the P_2 position as well (ligands **4e** and **f**). Based on the IC_{50} results, the affinity towards papain dropped by a factor three. These amino acids bear an extra CH_2 compared to phenylalanine and tyrosine. As a consequence of the longer side chain, the P_2 group is less optimal for binding into the S_2 subsite. This leads to the conclusion that the hydrophobic subpocket formed by Val133 and Val157 most comfortably accommodates the 4-azidomethylbenzoyl ligand **4c**.

2.3.4. Phenylbenzoyl ligands

As described by Löser et al. inhibitors featuring a biphenyl moiety, such as compound **2**, were found to display better affinity than the similar benzoylated ligand **1**.[13] However, in our experimental binding studies, inhibitors containing a biphenyl group that was 4′-substituted with an azidomethyl moiety, surprisingly displayed a significant decrease in binding affinity.

As depicted in Figure 5d and e, Tyr 61 andTyr67 move away to open up the binding site and to be able to fit the S_3 phenylbenzoyl group (**2** and **5b**). These docking poses do not provide an explanation for the loss in binding affinity after introduction of the azide moiety. It seems that the poses predicted by Fleksy allow too much flexibility in the S_3 pocket. From literature it is known that an alternative binding conformation can occur as well. Kim et al. showed a crystal structure for papain where the P_2 and P_3 residues are swapped and the P_3 group is now locked by the S_2 subsite.[25] This would give a better explanation for the fact that ligand **2** is a good binder, but that after introduction of the azide at the aromatic group the binding affinity drops, because the S_2 pocket is not large enough to accommodate the additional azide linker.

2.3.5. Leupeptin-based ligands

The third class of ligands that was evaluated are the leupeptin-based inhibitors **5a**–**c**. The experimentally determined IC_{50} values for these ligands were higher than for leupeptin or, for example, ligand **3c** (Table 1). The IC_{50} value of leupeptin was determined in the low nanomolar range (data not shown here). The

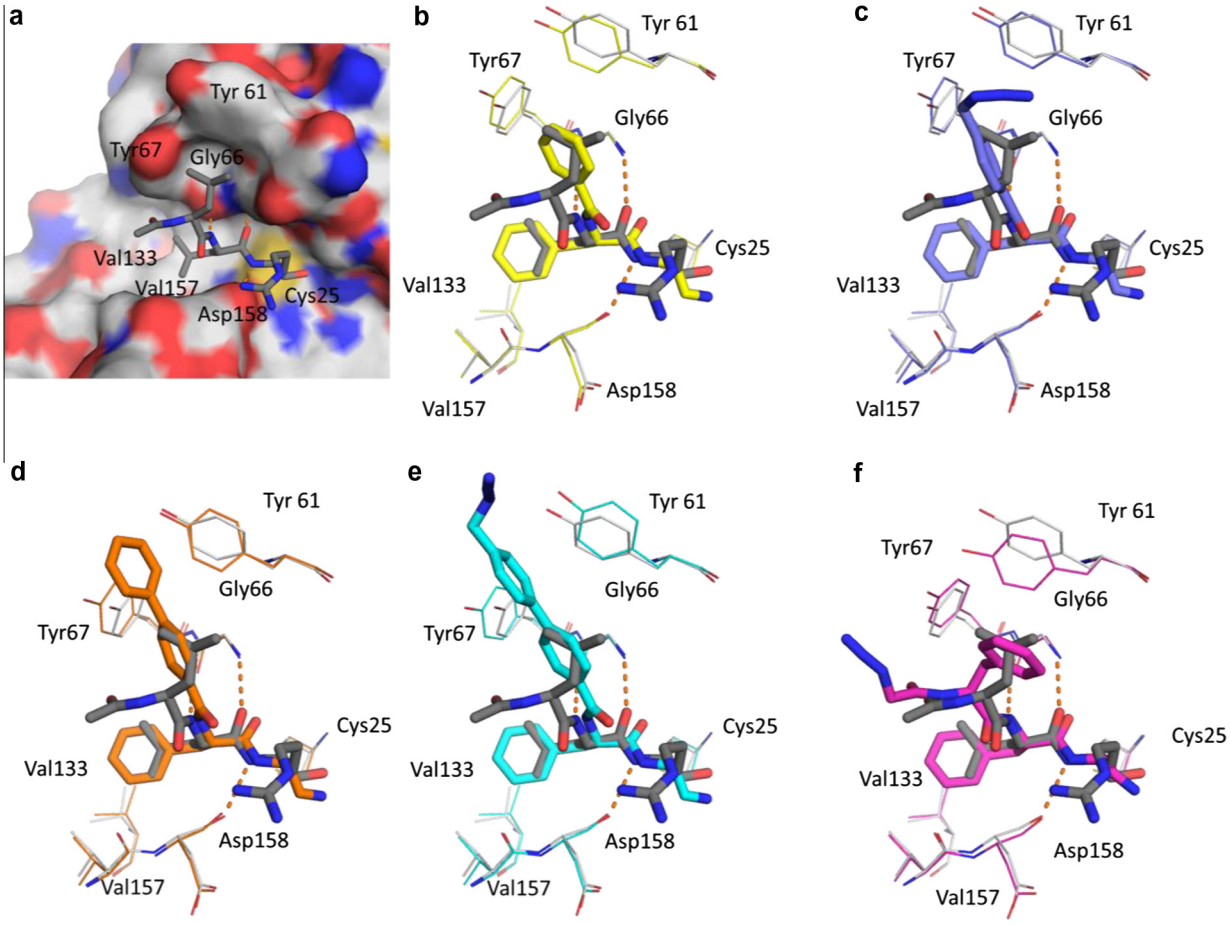

Figure 5. (a) Surface representation of PDB-code 1POP (C gray, O red, N blue, S yellow). The ligand leupeptin is covalently bound to Cys25 and forms three hydrogen bonds to the protein backbone of Gly66 and Asp156 (orange dashes). The hydrophobic S_2 binding site is formed by Val133 and Val157, while Tyr61 and Tyr67 form the S_3 binding site. Docking orientation of (b) benzoyl ligand **1** (yellow), (c) phenylalanine ligand **3c** (blue), (d) phenylbenzoyl ligand **2** (orange), (e) azidomethylated 4-phenylbenzoyl ligand **4b** (cyan) and (f) leupeptin-based ligand **5c** (pink), all superposed onto papain in complex with leupeptin (PDB code 1POP) (gray). For leupeptin, hydrogen bonds are shown (orange dashes).

Please cite this article in press as: Wammes, A. E. M.; et al. *Bioorg. Med. Chem.* (2014), http://dx.doi.org/10.1016/j.bmc.2014.06.001

leupeptin-based ligands did not contain the arginine of leupeptin at the P_1 position. With respect to the crystal structure 1POP the arginine group does not form additional hydrogen bonds to papain and therefore the impact on the binding affinity may be relatively small. Furthermore, the P_2 and P_3 groups are the same as for leupeptin or contain a phenylalanine, which outperformed other residues in terms of binding affinity in our other ligand series. Most likely the introduced azide moiety for ligands **5a–c** is not complementary in terms of interactions at the upper top of the S_2 subpocket (Tyr67), which would explain the significant loss in binding affinity.

3. Conclusions

In order to develop affinity-based biosensor platforms, appropriate ligands with a functional handle for immobilization onto a biosensor surface are required. To this end, a small library of enzyme inhibitors were designed and synthesized, containing different azide linkers for subsequent immobilization by 'click' chemistry, in this particular case by copper-free, strain-promoted azide–alkyne cycloaddition (SPAAC).

A robust and reproducible competitive UV assay was developed for evaluation of the inhibitory potential of the prepared ligands on papain. A satisfactory explanation of the observed IC_{50} values could not be given in all cases. To be able to properly interpret the results, a docking study was initiated in order to obtain more insight in the observed binding affinity values. Docking studies showed that ligands having a phenylalanine at the P_2 position can occupy the S_2 subsite best, which could explain the better IC_{50} value compared to the other ligands. For the phenylbenzoyl compounds a swapped binding mode was proposed where the P_2 aromatic group will bind into the S_3 subpocket and the P_3 phenylbenzoyl group will be locked by the S_2 subpocket. For the leupeptin-based ligands, the IC_{50} values showed a decrease in binding affinity. Based on the docking results, the introduced azide moiety for ligands **5a–c** is not complementary in terms of interactions at the upper top of the S_2 subpocket (Tyr67), which may explain the significant loss in binding affinity.

Although the azide handle is rather small, this moiety surprisingly strongly influenced the binding affinity of various compounds in the library. Therefore, generally it may be concluded that one should be careful when introducing immobilization handles to inhibitors. Furthermore, while the docking studies described here have only been used to understand the structure–activity relationships of existing compounds, the new insights will also be useful in the design of future compounds with improved inhibitory activity on papain.

4. Materials and methods

4.1. Synthesis

4.1.1. General

Reactions were followed and R_F values were obtained using thin layer chromatography (TLC) on silica gel-coated plates (Merck 60 F254) with the indicated solvent mixture. Detection was performed with UV light, and/or by charring at ~150 °C after dipping into a solution of either ninhydrin or Cl-TDM (bis[4-(dimethylamino)phenyl]methane). Melting points were analyzed with a Büchi melting point B-545. IR spectra were recorded on an ATI Mattson Genesis Series FTIR spectrometer, or a Bruker Tensor 27 FTIR spectrometer. NMR spectra were recorded on a Bruker DMX 300 (300 MHz), and a Varian 400 (400 MHz) spectrometer in $CDCl_3$ solutions (unless otherwise reported). Chemical shifts are given in parts per million (ppm) with respect to tetramethylsilane (TMS) as internal standard. Coupling constants are reported as J values in hertz. Peak assignment in ^{13}C spectra was based on 2D gHSQC and gHMBC spectra. Column or flash chromatography was carried out using Acros silica gel (0.035–0.070 mm, and ca. 6 nm pore diameter). Optical rotations were determined with a Perkin Elmer 241 polarimeter. High-resolution mass spectra were recorded on a JEOL AccuTOF (ESI), or a JEOL JMS-T100GCvAccTOF (EI and CI).

4.1.2. General procedure 1: Nitrile introduction

Under nitrogen atmosphere, Boc-AA-OH (1 equiv) was dissolved in dry THF and cooled to −25 °C. Subsequently, freshly distilled Et_3N (1 equiv) and isobutyl chloroformate (1 equiv) were sequentially added under vigorous stirring. After 30 min, a solution of aminoacetonitrile sulfate (1.1 equiv) in H_2O (0.5 mL), precooled on ice, and Et_3N (1 equiv) were added. The resulting mixture was allowed to warm to room temperature. After 2 h, THF was removed under reduced pressure and the residual aqueous mixture was diluted with a small volume of H_2O, adjusted to pH 1 (10% $KHSO_4$) and extracted with EtOAc. The combined organic layers were washed with H_2O, satd $NaHCO_3$ and brine, dried over Na_2SO_4 and evaporated to dryness. The solid residue was recrystallized.

4.1.3. General procedure 2: Boc deprotection

Trifluoroacetic acid (8 portions of 10 equiv) was added to a cold solution (0 °C) of Boc-$(AA)_n$-$NHCH_2CN$ (1 equiv) in H_2O/THF (1:1 v/v, 0.1 M). The mixture was stirred for 2 h at room temperature, after which the solvent was removed under reduced pressure and the reaction mixture was lyophilized to obtain the product.

4.1.4. General procedure 3: Amide coupling with EDC

To a cooled solution (0 °C) of $R'CO_2H$ (1.05 equiv) and H_2N-R'' (1 equiv) were added DMAP (2 equiv), HOBt (1 equiv) and EDC (1.05 equiv). The reaction mixture was allowed to warm up to room temperature and stirred for 16 h, after which the mixture was washed with $KHSO_4$, $NaHCO_3$ and brine, dried over Na_2SO_4 and concentrated in vacuo. The crude products were purified using column chromatography.

4.1.5. 4-(Azidomethyl)benzoyl-Leu-$NHCH_2CN$ (3a)

General procedure 3, using H-Leu-$NHCH_2CN$ (100 mg, 591 μmol) and CH_2Cl_2 (3 mL). The residue was purified using column chromatography (MeOH/CH_2Cl_2 1:19) yielding the product (77 mg, 40%) as colorless oil. R_F = 0.35 (MeOH/CH_2Cl_2 1:19). ^1H NMR (300 MHz, CD_3OD) δ = 7.89 (d, J = 8.3 Hz, 2H), 7.46 (d, J = 8.2 Hz, 2H), 4.64 (m, 1H), 4.45 (s, 2H), 4.17 (d, J = 1.9 Hz, 2H), 1.85–1.63 (m, 3H), 1.33 (t, J = 11.0 Hz, 1H), 0.99 (dd, J = 7.8, 6.2 Hz, 6H) ppm. ^{13}C NMR (75 MHz, CD_3OD) δ = 175.34, 169.94, 141.16, 134.89, 129.32, 128.78, 117.50, 54.99, 53.59, 41.58, 28.07, 26.15, 23.40, 21.90 ppm. FTIR = 3271, 3066, 2958, 2092, 1682, 1634, 15341, 1242 cm^{-1}. HRMS (ESI) calcd for $C_{16}H_{21}N_6O_2$ $(M+H)^+$ 329.1726, found 329.1745.

4.1.6. 4-(Azidomethyl)benzoyl-Nle-$NHCH_2CN$ (3b)

General procedure 3, using H-Nle-$NHCH_2CN$ (100 mg, 591 μmol) and CH_2Cl_2 (3 mL). The residue was purified using column chromatography (MeOH/CH_2Cl_2 1:49) yielding the product as slightly yellow crystals (132 mg, 68%). R_F = 0.35 (MeOH/CH_2Cl_2 1:19). ^1H NMR (300 MHz, $CDCl_3$) δ 7.87–7.79 (m, 2H), 7.40 (dd, J = 8.5, 2.5 Hz, 2H), 6.99 (m, 1H), 4.83–4.69 (m, 1H), 4.42 (d, J = 2.8 Hz, 2H), 4.16 (dd, J = 17.7, 5.7 Hz, 1H), 4.07 (dd, J = 7.6, 5.4 Hz, 1H), 2.10–1.92 (m, 1H), 1.92–1.71 (m, 1H), 1.42 (m, 4H), 0.92 (m, 3H) ppm. ^{13}C NMR (75 MHz, $CDCl_3$) δ 172.44, 172.31, 170.08, 167.50, 167.02, 139.85, 139.46, 133.79, 133.28, 130.77, 128.46, 128.38, 128.24, 128.11, 127.85, 115.94, 54.38, 54.28, 53.68, 53.58, 41.40, 32.46, 27.62, 22.62 ppm. FTIR = 3272, 2931,

2860, 2097, 1749, 1749, 1626, 1530, 1220, 672 cm^{-1}. HRMS (ESI) calcd for $C_{16}H_{20}N_6NaO_2$ $(M+Na)^+$ 351.1545, found 351.1563.

4.1.7. 4-(Azidomethyl)benzoyl-Phe-NHCH$_2$CN (3c)

General procedure 3, using H-Phe-NHCH$_2$CN (295 mg, 980 μmol) and EtOAc (10 mL). Column chromatography (MeOH/CH_2Cl_2 1:19) afforded the expected product (230 mg; 95%) as white crystals. Mp = 90–93 °C. R_F = 0.39 (MeOH/CH_2Cl_2 1:19). ^{1}H NMR (CD_3CN, 400 MHz) δ = 7.81–7.76 (m, 1H), 7.49–7.43 (m, 2H), 7.33 (m, 5H), 7.26 (m, 1H), 4.82 (m, 1H), 4.49 (s, 2H), 4.10 (dd, J = 5.9, 4.0 Hz, 2H), 3.35 (dd, J = 14.0, 5.2 Hz, 1H), 3.09 (dd, J = 13.9, 9.4 Hz, 1H) ppm. ^{13}C NMR (CD_3CN, 75 MHz) δ = 172.65, 167.54, 140.69, 138.51, 134.55, 131.01, 130.25, 129.41, 129.25, 128.67, 127.66, 118.31, 55.83, 54.62, 37.88, 28.22 ppm. FTIR = 3273, 3057, 2932, 2552, 2223, 2105, 1683, 1634, 1533, 1294, 1240 cm^{-1}. HRMS (ESI) m/z calcd for $C_{19}H_{19}N_6O_2$ $(M+H)^+$: 363.1579, found 363.1570.

4.1.8. 4-(Azidomethyl)benzoyl-Tyr-NHCH$_2$CN (3d)

General procedure 3, using H-Tyr-NHCH$_2$CN (90 mg, 456 μmol) and DMF (2 mL). Column chromatography (MeOH/CH_2Cl_2 1:19) afforded the expected product (86 mg, 50%) as yellow oil. R_F = 0.23 (MeOH/CH_2Cl_2 1:19). ^{1}H NMR (300 MHz, CD_3OD) δ = 7.78 (d, J = 8.1 Hz, 2H), 7.42 (d, J = 8.0 Hz, 2H), 7.11 (d, J = 8.4 Hz, 2H), 6.73 (d, J = 8.4 Hz, 2H), 4.74 (t, J = 7.5 Hz, 1H), 4.43 (s, 2H), 4.14 (d, J = 2.2 Hz, 2H), 3.17 (dd, J = 13.8, 6.5 Hz, 1H), 3.08–2.92 (m, 1H), 2.85 (s, 1H) ppm. ^{13}C NMR (75 MHz, CD_3OD) δ = 174.20, 169.67, 157.36, 141.09, 134.82, 131.32, 129.24, 128.95, 128.81, 117.31, 116.33, 56.87, 54.94, 37.90, 28.00 ppm. HRMS (ESI) m/z calcd for $C_{19}H_{18}N_6O_3Na$ $(M+Na)^+$: 401.1338, found 401.1349.

4.1.9. 4-(Azidomethyl)benzoyl-*h*-Phe-NHCH$_2$CN (3e)

General procedure 3, using H-*h*-Phe-NHCH$_2$CN (331 mg, 1.00 mmol) and DMF (10 mL). Column chromatography (MeOH/CH_2Cl_2 1:39) and recrystallization from EtOAc/Hept afforded the expected product (200 mg, 53%) as white crystals. Mp = 130–133 °C. R_F = 0.35 (EtOAc/Hept 1:1). ^{1}H NMR (400 MHz, CD_3CN) δ = 7.86 (d, J = 8.4 Hz, 2H), 7.46 (d, J = 8.6 Hz, 2H), 7.39 (d, J = 7.5 Hz, NH), 7.34 (s, NH), 7.31–7.16 (m, 5H), 4.50–4.42 (m, 3H), 4.49 (s, 2H), 4.05 (dd, J = 2.9, 5.8 Hz, 2H), 2.81–2.64 (m, 2H), 2.24–2.02 (m, 2H) ppm. ^{13}C NMR (75 MHz, CD_3CN) δ = 173.35, 167.96, 142.30, 140.68, 134.65, 129.47, 129.25, 128.91, 127.05, 117.86, 54.67, 54.46, 33.88, 32.72, 28.22 ppm. FTIR = 3266, 2220, 2103, 1671, 1631, 1531, 1497, 1239 cm^{-1}. HRMS (ESI) m/z calcd for $C_{20}H_{21}N_6O_2$ $(M+H)^+$: 377.1726, found 377.1731.

4.1.10. 4-(Azidomethyl)benzoyl-*h*-Tyr-NHCH$_2$CN (3f)

General procedure 3, using H-*h*-Tyr-NHCH$_2$CN (82 mg, 236 μmol) and DMF (3 mL). Column chromatography (EtOAc/Hept 1:1–3:1) afforded the expected product (41 mg, 44%) as white crystals. Mp = 48–50 °C. R_F = 0.45 (EtOAc/Hept 2:1). ^{1}H NMR (400 MHz, CD_3CN) δ 7.86 (d, J = 8.4 Hz, 2H), 7.47 (d, J = 8.6 Hz, 2H), 7.35 (d, J = 7.7 Hz, NH), 7.32 (d, J = 5.7 Hz, NH), 7.05 (d, J = 8.6 Hz, 2H), 6.72 (d, J = 8.6 Hz, 2H), 4.48 (s, 2H), 4.44 (ddd, J = 4.8, 7.6, 9.4 Hz, 1H), 4.05 (dd, J = 2.8, 5.8 Hz, 2H), 2.72–2.56 (m, 2H), 2.22–1.99 (m, 2H) ppm. ^{13}C NMR (75 MHz, CD_3CN) δ = 173.45, 167.95, 156.24, 140.67, 134.66, 133.20, 130.48, 129.24, 128.89, 116.18, 54.67, 54.44, 34.13, 31.80, 28.20 ppm. FTIR = 3296, 2976, 2930, 2101, 1639, 1535, 1515, 1244 cm^{-1}. HRMS (ESI) m/z calcd for $C_{20}H_{20}NaN_6O_3$ $(M+Na)^+$: 415.1495, found 415.1497.

4.1.11. 4-(Azidomethyl)biphenyl-Leu-NHCH$_2$CN (4a)

General procedure 3, using H-Leu-NHCH$_2$CN (6.3 mg, 37.4 μmol), carboxylic acid **13** (10 mg, 37.4 μmol) and DMF (1 mL). Prep-HPLC afforded the product as white crystals in 18% yield. ^{1}H NMR (300 MHz, $CDCl_3$) δ 7.87 (d, J = 8.6 Hz, 2H), 7.76–7.52 (m, 4H), 7.41 (d, J = 8.4 Hz, 2H), 4.78 (m, 1H), 4.40 (s, 2H), 1.75 (m, 1H), 1.61 (s, 2H), 0.99 (d, J = 4.5 Hz, 6H). ^{13}C NMR (75 MHz, $CDCl_3$) δ 184.93, 182.96, 174.04, 172.38, 167.26, 158.77, 146.60, 145.29, 144.03, 140.09, 135.44, 129.39, 128.94, 127.82, 127.43, 81.19, 74.03, 68.83, 46.70, 27.82. FTIR = 3292, 2957, 2098, 1756, 1631, 1533, 1495, 1212, 668 cm^{-1}.

4.1.12. 4-(Azidomethyl)biphenyl-Phe-NHCH$_2$CN (4b)

General procedure 3, using H-Phe-NHCH$_2$CN (100 mg, 315 μmol), carboxylic acid **13** (90 mg, 347 μmol) and DMF (10 mL). Column chromatography (MeOH/CH_2Cl_2 1:99) afforded the product as white crystals in 29% yield. ^{1}H NMR (400 MHz, CD_3OD) δ 7.85 (d, J = 8.7 Hz, 2H), 7.74–7.69 (m, 4H), 7.47 (dd, J = 2.0, 8.5 Hz, 2H), 7.33–7.19 (m, 5H), 4.82 (ddd, J = 6.3, 7.8, 8.9 Hz, 1H), 4.42 (s, 2H), 4.15 (s, 2H), 3.29–3.05 (m, 2H) ppm. ^{13}C NMR (75 MHz, CD_3OD) δ 174.08, 169.84, 145.23, 141.13, 138.34, 137.11, 133.95, 130.34, 130.06, 129.59, 129.17, 128.52, 127.98, 127.91, 117.32, 56.62, 55.20, 38.67 ppm. FTIR = 3426, 3369, 2945, 2090, 1758, 1690, 1640, 1533, 1198, 696 cm^{-1}. HRMS (ESI) m/z calcd for $C_{25}H_{22}N_6O_2Na$ $(M+Na)^+$: 461.1702, found 461.1693.

4.1.13. 4-(Azidomethyl)biphenyl-Tyr-NHCH$_2$CN (4c)

General procedure 3, using H-Tyr-NHCH$_2$CN (106 mg, 318 μmol), carboxylic acid **13** (96 mg, 350 μmol) and DMF (10 mL). Prep-HPLC afforded the product as white crystals in 14% yield. ^{1}H NMR (400 MHz, CD_3OD) δ 7.87 (d, J = 8.7 Hz, 2H), 7.75–7.68 (m, 4H), 7.47 (d, J = 8.4 Hz, 2H), 7.11 (d, J = 8.6 Hz, 2H), 6.72 (d, J = 8.6 Hz, 2H), 4.73 (t, J = 5.9 Hz, 1H), 4.42 (s, 2H), 4.15 (s, 2H), 3.22–2.93 (m, 2H) ppm. ^{13}C NMR (75 MHz, CD_3OD) δ 174.25, 157.43, 141.14, 137.10, 134.00, 131.35, 130.06, 129.17, 128.87, 128.52, 127.99, 117.32, 116.36, 56.91, 55.20, 37.97, 30.74, 28.01 ppm. FTIR = 3295, 2928, 2450, 2108, 1663, 1621, 1519, 1438, 1256, 1205, 1136 cm^{-1}. HRMS (ESI) m/z calcd for $C_{25}H_{22}N_6O_3Na$ $(M+Na)^+$: 477.1651, found 477.1644.

4.1.14. N_3CH_2CO-Leu-Leu-NHCH$_2$CN (5a)

General procedure 3, using H-Leu-Leu-NHCH$_2$CN·TFA (30·mg, 105 μmol). The residue was purified by column chromatography (MeOH/CH_2Cl_2 1:39) yielding the product (8 mg, 21%) as a slightly yellow gum. R_F = 0.39 (MeOH/CH_2Cl_2 1:19). ^{1}H NMR (300 MHz, CD_3OD) δ 4.37–4.47 (m, 2H) 4.42 (s, 2H), 3.91 (s, 2H), 1.29–1.70 (m, 6H), 0.95 (m, 12H) ppm. ^{13}C NMR (75 MHz, CD_3OD) δ 174.89, 174.63, 170.45, 117.40, 53.35, 52.88, 52.68, 48.15, 41.70, 41.50, 27.99, 25.86, 21.91, 20.96, 17.62, 16.55 ppm. HRMS (ESI) calcd for $C_{16}H_{27}N_7O_3$ $(M+H)^+$ 366.2254, found 366.2261.

4.1.15. N_3CH_2CO-Leu-Phe-NHCH$_2$CN (5b)

General procedure 3, using H-Leu-Phe-NHCH$_2$CN·TFA (76 mg, 240 μmol). The residue was purified by column chromatography (MeOH/CH_2Cl_2 1:19). The desired product (35 mg, 37% yield) was obtained as white/yellow crystals. R_F = 0.24 (MeOH/CH_2Cl_2 1:19). ^{1}H NMR (300 MHz, CD_3OD) δ 7.18–7.30 (m, 5H) 4.56 (t, J = 6 Hz, 1H), 4.36 (t, J = 6 Hz, 1H), 4.09 (s, 2H), 3.87 (s, 2H), 3.16 (dd, J = 9, 15 Hz, 1H), 2.97 (dd, J = 9, 15 Hz, 1H), 1.16–1.51 (m, 3H), 0.90 (m, 6H) ppm. ^{13}C NMR (75 MHz, CD_3OD) δ 174.31, 173.57, 170.46, 138.08, 130.35, 129.56, 127.87, 117.21, 55.90, 53.38, 52.58, 41.59, 38.41, 27.93, 25.79 ppm. HRMS (ESI) calcd for $C_{19}H_{25}N_7O_3$ $(M+H)^+$ 400.2097, found 400.2118.

4.1.16. N_3CH_2CO-Phe-Phe-NHCH$_2$CN (5c)

General procedure 3, using H-Phe-Phe-NHCH$_2$CN (40 mg, 89 μmol). The residue was purified by preparative HPLC. The desired product (39 mg, 70% yield) was obtained as white crystals. R_F = 0.30 (MeOH/CH_2Cl_2 1:19). ^{1}H NMR (400 MHz, CD_3CN) δ 7.28–7.14 (m, 10H), 4.56–4.47 (m, 2H), 4.06–3.98 (m, 2H), 3.85 (s, 1H),

3.77 (s, 2H), 3.16 (dd, J = 14.0, 5.3 Hz, 1H), 3.01 (dd, J = 14.0, 5.7 Hz, 1H), 2.90 (dd, J = 14.0, 8.8 Hz, 1H), 2.82 (dd, J = 14.0, 8.5 Hz, 1H) ppm. ^{13}C NMR (75 MHz, CD_3CN) δ 172.25, 171.58, 168.88, 138.11, 137.92, 131.47, 130.29, 129.39, 127.72, 125.25, 118.32, 117.59, 55.66, 55.18, 55.09, 52.37, 38.10, 28.27, 28.16 ppm. FTIR = 3282, 3066, 2923, 2850, 2409, 2102, 1639, 1542, 1453, 1259, 1030, 699 cm^{-1}. HRMS (ESI) calcd for $C_{22}H_{24}N_7O_3$ $(M+H)^+$ 434.1940, found 434.1961.

4.1.17. HO-biphenyl-CO_2Me (13)

To a solution of (4-bromophenyl)methanol (500 mg, 2.94 mmol) and [4-(methoxycarbonyl) phenyl]boronic acid (550 mg, 3.53 mmol) in DMF (20 mL) was added $Pd(OAc)_2$ (200 mg, 735 μmol) and Na_2CO_3 (3 g in 20 mL H_2O). The reaction mixture was allowed to stir at 70 °C. After 48 h, an extraction with EtOAc was performed; the organic layers were combined and washed with brine, dried over $MgSO_4$, filtrated and concentrated in vacuo. Column chromatography (EtOAc/Hept 1:4) yielded the product (170 mg, 24%) as white crystals. R_F = 0.3 (EtOAc/Hept 1:1). ^{1}H NMR (400 MHz, $CDCl_3$) δ 8.15–8.06 (m, 2H), 7.70–7.58 (m, 4H), 7.52–7.43 (m, 2H), 4.77 (d, J = 3.1 Hz, 2H), 4.07–3.67 (m, 3H), 1.75 (br s, 1H, OH) ppm. FTIR = 3305, 3032, 1718, 1604, 1432, 1399, 1286, 1271, 1220, 1111, 765 cm^{-1}. HRMS (EI) calcd for $C_{15}H_{14}O_3$ $(M)^+$ 242.0942, found 242.0919.

4.1.18. Azidomethyl-biphenyl-CO_2Me (14)

To a cold solution (0 °C) of HO-biphenyl-CO_2Me (100 mg, 412 μmol) in CH_2Cl_2 (5 mL) was added Et_3N (86 μL, 618 μmol) and MsCl (35 μL, 453 μmol). The reaction was allowed to stir at room temperature and after full conversion was seen on TLC (16 h), the mixture was quenched with H_2O, extra CH_2Cl_2 was added and the organic layer was washed with water, brine, dried over $MgSO_4$, filtrated and concentrated in vacuo. The crude product was redissolved in DMF and NaN_3 (200 mg, 3.08 mmol) was added. The reaction mixture was stirred for 16 h, H_2O was added and the mixture was extracted three times with EtOAc, dried over Na_2SO_4, filtrated and concentrated in vacuo. Column chromatography (EtOAc/Hept 1:4) yielded the product (108 mg, 98%) as white crystals. R_F = 0.8 (EtOAc/Hept 1:1) ^{1}H NMR (400 MHz, $CDCl_3$) δ 8.03 (d, J = 8.6 Hz, 2H), 7.55 (dd, J = 12.9, 8.5 Hz, 4H), 7.40 (d, J = 8.4 Hz, 2H), 4.41 (s, 2H), 3.86 (s, 3H) ppm. ^{13}C NMR (101 MHz, $CDCl_3$) δ 166.89, 144.82, 140.09, 140.08, 137.39, 130.13, 129.16, 129.13, 127.60, 126.99, 77.34, 77.02, 76.70, 52.14, 45.82, 31.87, 22.68, 14.10, 1.01 ppm. FTIR = 2958, 2843, 2105, 1719, 1608, 1432, 1397, 1286, 1110, 768, 736 cm^{-1}. HRMS (EI) calcd for $C_{15}H_{13}N_3O_2$ $(M-N_3)^+$ 225.0915, found 225.0896.

4.1.19. Azidomethyl-biphenyl-CO_2H (10)

To a solution of azidomethyl-biphenyl-CO_2Me (108 mg, 404 μmol) was added THF (500 μL) and 1.5 mL 1 M NaOH. The mixture was allowed to stir for 16 h, extracted with EtOAc, washed with brine, dried over $MgSO_4$, filtrated and concentrated in vacuo. Lyophilization afforded the product in quantitative yield as white crystals. ^{1}H NMR (300 MHz, CD_3OD) δ 8.22–7.93 (m, 2H), 7.83–7.50 (m, 4H), 7.35 (m, 2H), 4.36 (s, 2H) ppm. FTIR = 2959, 2922, 2852, 2672, 2549, 2098, 1671, 1706, 1607, 1428, 1292, 737 cm^{-1}. HRMS (ESI) calcd for $C_{14}H_{10}N_3O_2$ $(M-H)^-$ 252.0760, found 252.0787.

4.1.20. DIBAC triazole 18

To a solution of nitrile **3c** (3.2 mg, 8.90 μmol) in 0.5 mL MeOH was added DIBAC (4 mg, 8.90 μmol) and the mixture was allowed to stir for 1 h, after which full conversion was seen. The product was concentrated in vacuo, purified with HPLC (C18 column, gradient eluent: 5–100% acetonitrile/H_2O + 0.1%TFA) and finally, lyophilization afforded the expected product as white crystals (unseparable 1:1 mixture of triazole regioisomers, 5.1 mg, 70%). ^{1}H NMR (300 MHz, CD_3OD) δ 7.78–7.04 (m, 17H), 4.47–4.49 (m, 1H), 4.43 (s, 2H), 4.14 (s, 2H), 3.60 (s, 2H), 3.60–3.47 (m, 5H), 3.24–3.26 (m, 1H), 3.11–3.06 (dd, 1H, J = 13.7, 8.9), 2.84–2.79 (m, 1H), 1.89–1.82 (m, 3H), 1.62–1.48 (m, 2H), 1.36–1.29 (m, 3H), 0.97–0.87 (m, 2H) ppm. HRMS (ESI) calcd for $C_{45}H_{50}N_9O_6$ $(M+H)^+$ 812.3884; found 812.3906.

4.2. Enzymatic assay

Enzyme activities were calculated from kinetic measurements performed by spectrophotometric detection of the product 4-nitroaniline (pNA) at 25 °C in a 1 mm cuvette at a wavelength of 380 nm. A 4.5 mM stock solution of the chromogenic substrate Z-Phe-Arg-pNA was prepared in DMSO; the final concentration was 300 μM. Stock solutions of the inhibitors were also prepared in DMSO and final concentrations were in a range from 10 nM to 100 μM. In the absence of inhibitor, 20 μL of DMSO was added to the cuvette. The final papain concentration used in the assay was 100 nM.

For daily activation of papain, a 10 μM solution was prepared in a 0.1 M sodium phosphate buffer (pH 6.5), containing 2.5 mM EDTA and 15 mM DTT (activation buffer). The solution was incubated at 25 °C for 1 h and the activated enzyme was kept on ice. In this way stability was ensured for 6–8 h. Further dilutions were made in a 0.1 M sodium phosphate buffer (pH 6.5), containing 2.5 mM EDTA, 300 μM DTT and 6% DMSO (running buffer).

After thermal equilibration, the reaction was initiated by addition of the enzyme and progress curves were monitored over 7–10 min. The initial velocities (V_{ini}) were determined for seven different inhibitor concentrations in triplicate.

4.3. Molecular docking

4.3.1. Small molecule preparation

With the modeling package MOE (2011.10)[26] from CCG 3D structures of the inhibitors were drawn and energy minimized.

4.3.2. Docking

All molecular docking studies in papain were performed using the flexible docking program Fleksy (1.2.3) with default settings.[22] The crystal structure of a papain–leupeptin complex (PDB entry 1POP) was used for all docking studies.[21] The docking process and protocol in Fleksy was based on FlexX technology, as explained in detail by Nabuurs et al.[22] The docking algorithm of FlexX cuts ligands into fragments. One of those fragments was placed into the binding site and the rest of the ligand was systematically added. All steps were scored and only the best scored poses were further considered.

Covalent docking with Fleksy is not directly possible. In order to simulate a covalent docking in Fleksy the position of the first fragment (base fragment) placed during the docking process was locked. Here, the base fragment was provided in form of the C-terminal amide bond of the inhibitors (Fig. 3, red part of structure) to simulate a covalent docking protocol.

4.3.3. Structural alignment

The papain structures (1BP4, 1BQI, 1CVZ, 1KHP, 1KHQ, 1PAD, 1PE6, 1PIP, 1POP, 1PPD, 1PPN, 1PPP, 1STF, 2CIO, 2PAD, 3E1Z, 3IMA, 3LFY, 3TNX, 4PAD, 5PAD, 6PAD, 9PAP) were aligned based on the position of their Cα atoms in PyMol.

Acknowledgments

This work was financed by the INTERREG IV A Germany–Netherlands program through EU funding from the European

Regional Development Fund, the MWEBWV Ministry of North-Rhine Westphalia, the Dutch Ministry of Economic Affairs, Province of Gelderland and the project management Euregio Rhein-Waal.

References and notes

1. Diamond, D. *Principles of Chemical and Biological Sensors*; John Wiley and Sons: New York, 1998.
2. Saha, K.; Agasti, S. S.; Kim, C.; Li, X. N.; Rotello, V. M. *Chem. Rev.* **2012**, *112*, 2739.
3. Schasfoort, R. B. M.; Tudos, A. J. *Handbook of Surface Plasmon Resonance*; RSC: Cambridge, UK, 2008.
4. Debets, M. F.; van Berkel, S. S.; Dommerholt, J.; Dirks, A. T.; Rutjes, F. P. J. T.; van Delft, F. L. *Acc. Chem. Res.* **2011**, *44*, 805.
5. Debets, M. F.; van Berkel, S. S.; Schoffelen, S.; Rutjes, F. P. J. T.; van Hest, J. C. M.; van Delft, F. L. *Chem. Commun.* **2010**, 97.
6. Debets, M. F.; van der Doelen, C. W. J.; Rutjes, F. P. J. T.; van Delft, F. L. *ChemBioChem* **2010**, *11*, 1168.
7. Agard, N. J.; Prescher, J. A.; Bertozzi, C. R. *J. Am. Chem. Soc.* **2004**, *126*, 15046.
8. Dommerholt, J.; Schmidt, S.; Temming, R. P.; Hendriks, L. J.; Rutjes, F. P. J. T.; van Hest, J. C. M.; Lefeber, D. J.; Friedl, P.; van Delft, F. L. *Angew. Chem., Int. Ed.* **2010**, *49*, 9422.
9. Wammes, A. E. M.; Fischer, M. J. E.; de Mol, N. J.; van Eldijk, M. B.; Rutjes, F. P. J. T.; van Hest, J. C. M.; van Delft, F. L. *Lab Chip* **2013**, *13*, 1863.
10. de Beer, R. J. A. C.; Bogels, B.; Schaftenaar, G.; Zarzycka, B.; Quaedflieg, P. J. L. M.; van Delft, F. L.; Nabuurs, S. B.; Rutjes, F. P. J. T. *ChemBioChem* **2012**, *13*, 1785.
11. de Beer, R. J. A. C.; Zarzycka, B.; Amatdjais-Groenen, H. I. V.; Jans, S. C.; Nuijens, T.; Quaedflieg, P. J. L. M.; van Delft, F. L.; Nabuurs, S. B.; Rutjes, F. P. J. T. *ChemBioChem* **2011**, *12*, 2201.
12. de Beer, R. J. A. C.; Zarzycka, B.; Mariman, M.; Amatdjais-Groenen, H. I. V.; Mulders, M. J.; Quaedflieg, P. J. L. M.; van Delft, F. L.; Nabuurs, S. B.; Rutjes, F. P. J. T. *ChemBioChem* **2012**, *13*, 1319.
13. Löser, R.; Schilling, K.; Dimmig, E.; Gutschow, M. *J. Med. Chem.* **2005**, *48*, 7688.
14. Storer, A. C.; Menard, R. *Perspect. Drug Discov.* **1996**, *6*, 33.
15. Leung-Toung, R.; Li, W.; Tam, T. F.; Karimian, K. *Curr. Med. Chem.* **2002**, *9*, 979.
16. Otto, H. H.; Schirmeister, T. *Chem. Rev.* **1997**, *97*, 133.
17. Shaw, E. *Adv. Enzymol. RAMB* **1990**, *63*, 271.
18. Wieczerzak, E.; Drabik, P.; Lankiewicz, L.; Oldziej, S.; Grzonka, Z.; Abrahamson, M.; Grubb, A.; Bromme, D. *J. Med. Chem.* **2002**, *45*, 4202.
19. Foot, J. S.; Lui, F. E.; Kluger, R. *Chem. Commun.* **2009**, 7315.
20. Schechter, I.; Berger, A. *Biochem. Biophys. Res. Commun.* **1967**, *27*, 157.
21. Schröder, E.; Phillips, C.; Garman, E.; Harlos, K.; Crawford, C. *FEBS Lett.* **1993**, *315*, 38.
22. Nabuurs, S. B.; Wagener, M.; De Vlieg, J. *J. Med. Chem.* **2007**, *50*, 6507.
23. Koshland, D. E. *Proc. Natl. Acad. Sci. U.S.A.* **1958**, *44*, 98.
24. All used PDB-entries and their codes: BP4B, 1CVZ, 1KHP, 1KHQ, 1PAD, 2PAD, 4PAD, 5PAD, 6PAD, 1PE6, 1PIP, 1POP, 1PPD, 1PPN, 1PPP, 1STF, 2CIO, 3EIZ, 3IMA, 3LFY, 3TNX, 9PAP.
25. Kim, M. J.; Yamamoto, D.; Matsumoto, K.; Inoue, M.; Ishida, T.; Mizuno, H.; Sumiya, S.; Kitamura, K. *Biochem. J.* **1992**, *287*, 797.
26. Molecular Operating Environment (MOE), 2011.10. Chemical Computing Group Inc, 1010 Sherbooke St. West, Suite #910, Montreal, QC, Canada.